Study of Mechanical Models of the Single Aperture 11 T Nb_3Sn Dipole

I. Novitski, N. Andreev, B. Auchmann, E. Barzi, R. Bossert, M. Karppinen, A. Nobrega, D. Smekens, A.V. Zlobin

***Abstract*— Fermilab and CERN have a joint R&D program with the goal of building a 5.5-m long twin-aperture Nb_3Sn dipole magnet suitable for installation in the LHC. The first step of this program is the development of a 2-m long single-aperture demonstration dipoles with the nominal field of 11 T at the LHC nominal current of ~11.85 kA and 60 mm bore with ~20% margin. Prior to the construction of the real model magnets, shorter sections of the magnet straight part were assembled and instrumented with strain gauges to validate the results of FE structural analysis and to gain experience with the assembly of the real magnet components. This paper summarizes the lessons learned from these mechanical models and compares the measured data with the FEA.**

***Index Terms*— superconducting accelerator magnets, finite element analysis (FEA), mechanical model, strain gauges.**

I. Introduction

The LHC collimation system upgrade will allow particle beam operation at nominal and ultimate intensities. It foresees additional collimators to be installed in the dispersion suppressor areas and around high luminosity interaction regions [1]. In those areas several 14.3 m long 8.33 T LHC main dipoles (MB) will be replaced with 3.5 m collimators and two 5.5 m long 11 T dipoles. These twin-aperture dipoles operating at 1.9 K will be powered in series with the main dipoles and deliver the same integrated strength of 119 Tm at the nominal current of 11.85 kA. To demonstrate feasibility of this approach, CERN and FNAL have started a joint program to build a 5.5 m long twin aperture Nb_3Sn dipole for the collimation system upgrade. The first step of this program is the design and construction of a 2 m long single-aperture demonstrator magnet with a 60 mm bore, an 11 T field at the LHC nominal current of 11.85 kA and 20% margin [2].

Prior to the construction of the real model magnets, shorter sections of the magnet straight part were assembled and instrumented with strain gauges to validate the results of FE structural analysis, check tooling and to gain experience with the assembly of the real magnet components. This paper summarizes the lessons learned from these mechanical models based on integrated coil poles and compares the measured data with the finite element analysis (FEA).

Manuscript received October 9, 2012. Work supported by Fermi Research Alliance, LLC, under contract No. DE-AC02-07CH11359 with the U.S. Department of Energy and European Commission under FP7 project HiLumi LHC, GA no.284404.

N. Andreev, E. Barzi, R. Bossert, F. Nobrega, I. Novitski, A.V. Zlobin are with Fermi National Accelerator Laboratory, P.O. Box 500, Batavia, IL 60510, USA, (phone: 630-840-4823; fax: 630-840-8079; e-mail: novitski@fnal.gov).

B. Auchmann, M. Karppinen, D. Smekens are with the the European Organization for Nuclear Research, CERN CH-1211, Genève 23, Switzerland.

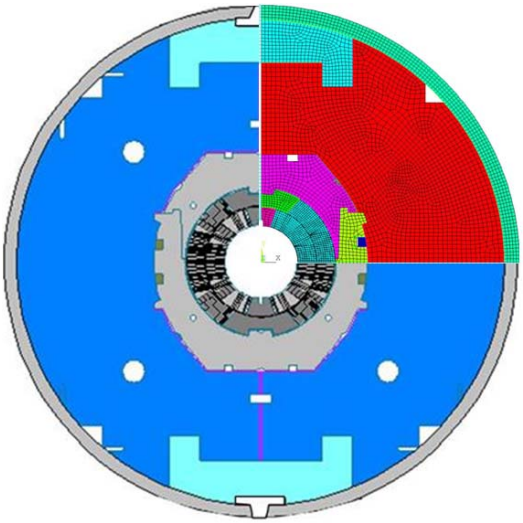

Fig. 1. Magnet cross-section with integrated FEA model.

II. Magnet Design

A. Design Concept

Details of the 11 T demonstrator dipole design are reported in [3]. The cross-section of the demonstrator dipole cold mass is shown in Fig. 1. The coil consists of 56 turns, 22 in the inner layer and 34 in the outer layer. Each coil is wound using a 40 strand Rutherford Nb_3Sn cable [4] insulated with two layers of E-glass tape 0.075 mm thick and 12.7 mm wide. The cable is made of RRP-108/127 strands 0.7 mm in diameter with a nominal Jc (12T, 4.2K) of 2750 A/mm2, a nominal Cu fraction of 0.53, and RRR>60. The reacted and epoxy-impregnated coils are surrounded by ground insulation made of 5 layers of 0.125 mm thick Kapton, stainless steel protection shells and laminated collars. The collared coil assembly is placed inside two half-yokes locked with Al clamps. The stainless steel skin is pre-tensioned and welded to obtain a coil pre-stress, sufficient to keep it under compression up to the full design field of 12 T.

B. FEA Goals and Results

The goal for the mechanical design is to provide a stable geometry of the conductor turns. Rigid turn positioning reduces the probability of spontaneous quenches due to conductor motion and stabilizes the magnet field harmonics. This stability is achieved by applying pre-stress to the coil during magnet assembly and supporting the compressed coil with a rigid structure during the operation.

TABLE I.
FEA RESULTS OF THE DIPOLE MECHANICAL STRUCTURE

Position in coil	Azimuthal Coil Stress, MPa		
	Collared coil	Clamped yoke	Cold mass
Inner pole	-44	-60	-120
Outer pole	-64	-55	-87
Inner middle plane	-97	-58	-79
Outer middle plane	-51	-55	-108

The 2D parametric ANSYS model has been used to analyze the mechanical characteristics of the dipole design at several magnet stages: magnet assembly at room temperature (collaring, yoke clamping and skin welding), cool-down to operation temperature, and excitation to the nominal current of 11.85 kA. The mechanical structure and the coil pre-stress were optimized to maintain the coils under compression up to the ultimate design field of 12 T and to keep the coil stress below 165 MPa. In the FE model, the coil middle plane and radial shims create initial coil azimuthal and radial pre-stress at collaring stage. Then midplane collar-yoke shims, skin and clamp tensions deform the iron, reduce the vertical collars spring-back and finalize coil compression. Strong collars and iron yoke create the "rigidity belt" around the Nb_3Sn coil to protect conductor from over-compression. Collar-yoke-clamp-skin interferences support the large horizontal Lorentz force. The results of the FEA of the demonstrator dipole mechanical structure at room temperature are shown in Table I.

III. MECHANICAL MODELS

Several versions of the instrumented mechanical model (MM) were built to verify the magnet design concept, measure stresses in the structural components, and validate the FEA results. The major goal for the MM was to develop a recommendation for real magnet assembly by finalizing the coil and yoke shim plans, and collaring and yoke clamping procedures.

The first 2 m practice coil was cut into four pieces and used in these models for the straight magnet section and for the ends. Fig. 2 shows two coil straight sections.

Fig. 2. Two instrumented central sections used for mechanical model assemblies shown from top and bottom.

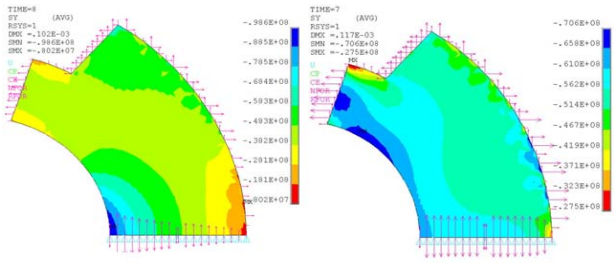

Fig. 3. Azimuthal stress distribution in Nb_3Sn coil composite.

The potted coil consists of Nb_3Sn conductors, titanium poles, stainless steel wedges and insulation (similar to G10). The FEA model simplifies coil properties by using cold elastic module of the conductor-insulation composite. The differences between warm and cold coil properties and the anisotropy in azimuthal and radial directions are well known facts [5]. For these reasons actual magnet shim sizes will be different from calculated ones. These shims need to be optimized using the MM to achieve the desired warm coil pre-stress as shown on Fig. 3.

A. *Coil Instrumentation*

A set of resistive strain gauges glued to the different parts of the potted coil were used for stress measurements during mechanical model assembly. The gauges on the coil's inner surface were located next to the gauges on the stainless steel wedges and on the titanium poles for cross-checking (see Fig. 4). A layer of coil ground insulation was substituted with compressive Fuji Film to measure a stress gradient on coil-coil and coil-collar contact surfaces.

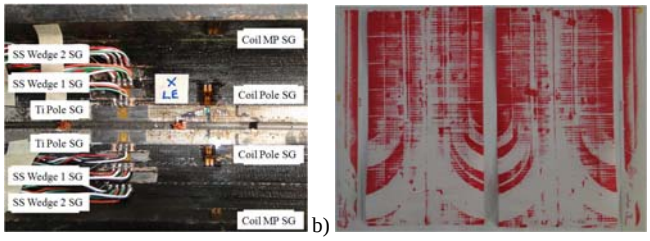

Fig. 4. Strain gauges map on the inner coil surface (a) and Fuji Film imprint of coil OD after end model assembly (b).

B. *Size Control*

The amount of applied stress to the coils depends on the coil size and collar cavity dimensions. The deviations of coil outer diameter (OD) and midplane from the design values were measured using a 3D Cordax device. The results of measurements in free stages are shown on Fig. 5a.

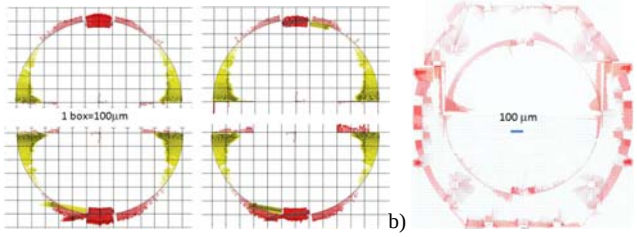

Fig. 5. Size deviation of two paired coils at two instrumented locations (a) and individual lams geometry profile (b).

The collar lams profile after laser cutting is shown on Fig. 5b. The collar size measurements were performed on the optical table. All collar laminations had the same orientation in one welded collar pack mirroring lam's production layout. Each pack is 380 mm long to achieve axial rigidity. The packs relative orientation was chosen (diagonal witness mark position) based on Fuji Film results with better uniformity of the coil radial pressure. The inner diameter (ID) of the assembled and keyed collar packs was also measured with micrometer to confirm Cordax data. The accuracy of wire-cut 25 mm thick yoke laminations is within +/-25 μm on all working surfaces.

C. Coil and Yoke Shimming

There are two places for the coil shimming inside the collar packs. They are shown in Fig. 6: azimuthal shim in the midplane between two coils and radial shim between coil and collar. The collar-yoke flat and tapered shim dimensions for the MM yoking are also shown. Coil poles are not shimmed in this case since they are integrated into potted coil structure.

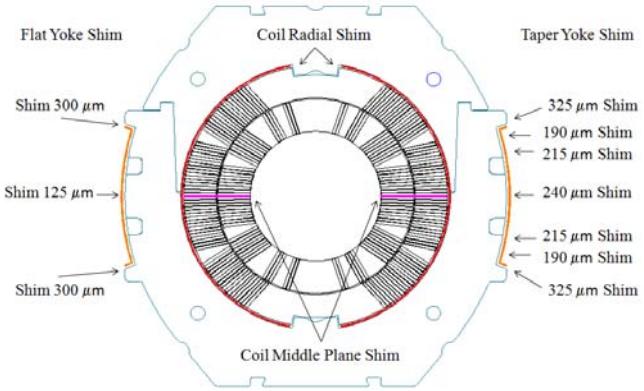

Fig. 6. Shim location inside the collar packs and size of two shims for the yoke: flat on the left and tapered on the right.

The final coil stress distribution should be similar to that predicted by FEA; however, the way to achieve it depends on the plastic coil deformation during magnet assembly and the coil-collar interface profile. Based on the coil and collar pack sizes the coil–collar interface has to be shimmed for a better roundness. It forced us to study the effect of the coil radial shim size on the coil stress distribution. From the FEA we know that the radial shim works more effectively for the pole turn compression than the middle plane shim, but increases the coil maximum stress. Since coil and yoke shims act together, an increase of the coil radial shim may reduce the yoke shim and decrease collared coil oval-shape after yoke clamping. A decision was made to change the radial shim as a main parameter for the mechanical models. Table II shows different coil shimming used for MM collaring.

TABLE II.
COIL SHIMMING

MM	#1	#2	#3	#4	#5	#6	#7end	FEA
Coil middle plane	0	0	75	75	75	75	75	100
Coil radial	0	75	100	125	225	175	175	25

D. Collaring Procedure

Collaring is the first loading step, when the impregnated coils are compressed for the first time by horizontal press within the collars and tooling defined boundaries. Fig. 7 shows collar pack assembly around shimmed coils and model placement in collaring tooling.

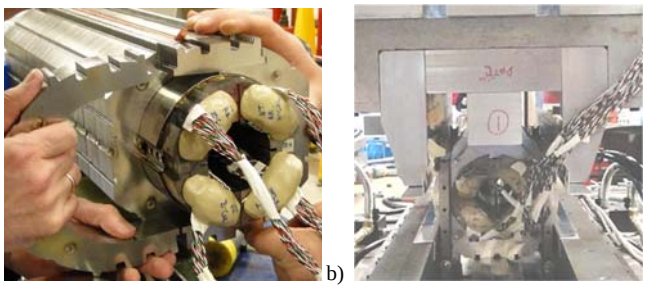

Fig. 7. Collar packs assembly around shimmed coils (a) and model placement into collaring tooling (b).

After locking the collar with keys, the pressure was released, tooling removed, and the compressed coil relaxed (sprig-back effect). Table III shows changes in the outside collar geometry (collar deflections) indicating the final coil stress level.

TABLE III.
COLLAR RADIAL DEFLECTION AT STRAIGHT SECTION

MM	#1	#4	#5	#6	#7	#7end	FEA
At coil middle plane	10	7	67	43	62	24	20
At coil pole	64	58	79	52	71	33	86

To minimize Nb_3Sn coil stress and collared coil spring-back, a special multi-step collaring procedure was developed [6]. The tapered keys are pushed into the keyways gradually with a 1-2 mm step. This allows controlling the stress increase in the compressed area of the Nb_3Sn coils. In this case, knowing coil plastic properties becomes very important. For simplicity, an assumption of 20 GPa for the coil elastic modulus has been made for that region. The SG history of four collared-coil mechanical models is shown in Fig. 8.

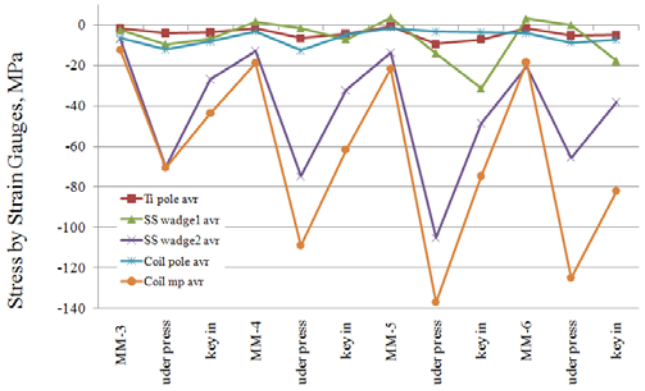

Fig. 8. SG history of four mechanical models loading. Each model has three readings: before compression, at maximum press load and after key insertion.

Each model has three readings: before compression, at maximum press load, and after key insertion. The maximum

pick stress in the coil is located at the inner layer parting plane and illustrated by SG readings located at the coil middle plane. The SG data for the coil pole turns and for the Ti poles, as well as the data for the coil middle plane turns and for the stainless steel wedges match each other reasonably well. Stress distribution in the coil is similar to the FEA picture.

The MM#6 shimming was selected for the magnet based on better matching of gauges date with FEA prediction, and radial pressure distribution from Fuji Film. The coil's and collar's dimensions deviate from the design value and have an effect on the final shim choice.

E. Yoking Procedure

The yoke clamping is the second assembly step. The collared coils were rotated by 90 degree and compressed under the press with two iron yokes. The two yokes were locked by the insertion of two aluminum side clamps and press load was released. As a result, the coils were deformed into a small vertical ellipse by shims placed between the clamped iron and the collars. The mechanical model iterated with two shim sizes shown in Fig. 6 and Fig. 9.

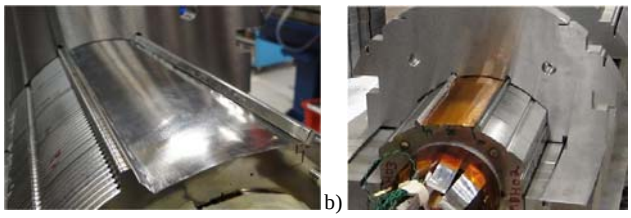

Fig. 9. Collar-yoke shim for two iterations of yoke clamping: 125 um flat (a) and 240 um tapered (b).

The collared coils with the same coil's shimming (from MM#6) were clamped two times. During clamping, the press load was applied gradually. The full system motion was monitored using control spacers and dial indicators. It helps to manage the gradual coil stress increase. The final stage of iron yoke clamping is shown on Fig.10.

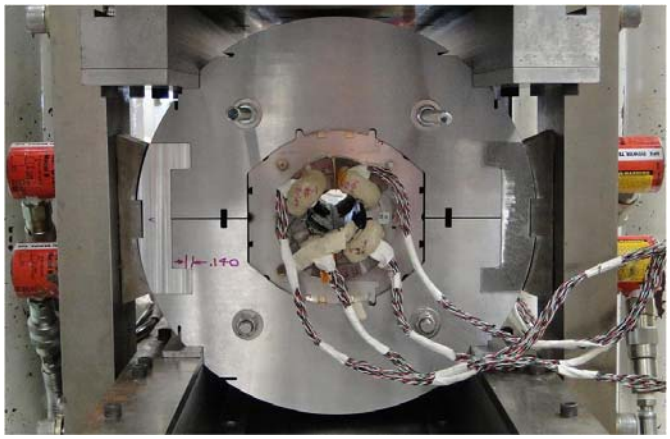

Fig. 10. The final stage of iron yoke clamping.

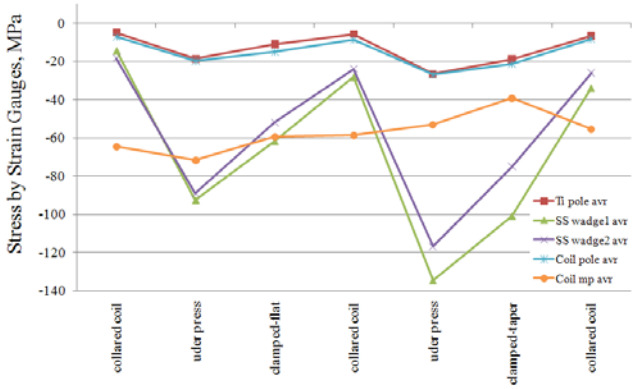

Fig. 11. SG history of two clamping iterations with two collar-yoke shims: flat-125um (first 3 points) and tapered-240um.

The SG history of two clamping runs is plotted on Fig. 11. Each iteration has readings at maximum press load (under press) and after clamp insertion (clamped). The coil pick stress moved from the coil middle plane turn to the coil inner pole location as expected from FEA. The pole turns load increases with bigger shim size but remains below 165 MPa. The tapered shim was selected for the magnet due to a better matching of gauges data with FEA prediction. Multiple compressions of the same Nb_3Sn coils were also counted.

IV. Conclusion

Several versions of the instrumented mechanical model have been built prior to the construction of the real dipole model to verify magnet design concept, measure stresses in the structural components, and to validate FEA results. Based on the MM test results, the coil and yoke shim plans, the collaring and yoke clamping procedures have been developed for the 11 T demonstrator dipole.

Acknowledgment

The authors would like to thank the technical staff of Fermilab's Technical Division for their contribution to models fabrication and testing.

References

[1] L. Bottura et al., "Advanced Accelerator Magnets for Upgrading the LHC", *IEEE Trans. on Appl. Supercond., vol. 22, June* 2012.

[2] A.V. Zlobin et al., "Development of Nb_3Sn 11T Single Aperture Demonstrator Dipole for LHC Upgrades", Fermilab-Conf-11-126-TD, PAC'2011, NYC, March 2011.

[3] A.V. Zlobin et al., "Design and Fabrication of a Single-Aperture 11T Nb3Sn Dipole Model for LHC Upgrades", *IEEE Trans. on Appl. Supercond.*, 2012.

[4] E. Barzi et al., "Development and Fabrication of Nb_3Sn Rutherford Cable for the 11 T DS Dipole Demonstration Model", *IEEE Trans. on Appl. Supercond.*, 2012.

[5] D. R. Chichili, et al., "Investigation of cable insulation and thermo-mechanical properties of epoxy impregnated Nb Sn composites," *IEEE Trans. Appl. Superconduct.*, vol. 10, Mar. 2000

[6] R.C. Bossert et al., "Fabrication and Test of 90 mm Nb_3Sn Model Based on Dipole Type Collar", *presented at ASC2010*, Washington, DC, 2010.